Progress Report: Multiscale Phase Inversion of Anisotropic Data

Shihang Feng[1]
[1]King Abdullah University of Science and Technology (KAUST)

ABSTRACT

In this paper, we extend the multiscale phase inversion (MPI) methodology to anisotropic media. The MPI method is developed to avoid the cycle-skipping problem of full waveform inversion (FWI) by temporally integrating the traces several times. The inversion of v_{p0} with a fixed ϵ is initially performed using the multiscale method. Numerical tests on synthetic data demonstrate the feasibility of this method.

INTRODUCTION

Conventional full waveform inversion (FWI) inverts for a velocity model by using an objective function that minimizes the L2 norm of the residuals between the predicted and the observed traces (Tarantola, 2005; Virieux and Operto, 2009). However, such a misfit function is highly non-linear and the iterations often get stuck in a local minimum.

In order to mitigate this problem, a skeletonized representation of the data such as first-arrival traveltimes (Luo and Schuster, 1991a,b; Zhou et al., 1995) can be inverted to obtain the low-to-intermediate wavenumber details of the background velocity model. The misfit function for skeletonized inversion is quasi-linear and enjoys better convergence properties than conventional FWI. The resulting tomograms provide a good starting model for FWI and reduce the likelihood of cycle skipping. However, refraction arrivals only provide the low-intermediate wavenumber information of the shallow part of the model. In order to reach deeper depth, the inversion methods has been extended to reflection waves, such as reflection WT (Ma and Hale, 2013; Shihang et al., 2017) and migration velocity analysis (MVA) (Sava et al., 2005; Sava and Vlad, 2008). However, it is still challenging to invert the velocity distribution with the complex geology such as salt dome.

As an alternative, multiscale strategy can also mitigate the cycle skipping problem of FWI (Bunks et al., 1995). Conventional multiscale FWI apply a low-pass filter on the data, so the objective function enjoy less local minimals. The drawback of this method is that sometimes low frequency components are weaker than the high frequency components.

To combine the multiscale strategy and skeletonized inversion, Sun and Schuster (1993) develop multiscale phase inversion method, where the recorded data are integrated several times in the time domain to boost the low-frequency components. This method had been successfully applied to crosswell data (Sun and Schuster, 1993) and surface seismic data with isotropic media (Fu et al., 2017). In this paper, we extend the multiscale phase inversion methodology to anisotropic media.

After the introduction, the next section of this paper summarizes the theory of this method, and the workflow is in the third section. Numerical tests on synthetic data are shown in the following section and the conclusions are in the last section.

THEORY

Multiscale phase inversion can be extended to VTI medium by inverting for the anisotropy parameters v_{p0}, ϵ and δ using the MPI misfit function,

$$\begin{aligned}\zeta &= \frac{1}{2}\sum_{s,g}\int dt\left[I^n\bar{d}(\mathbf{g},t|\mathbf{s}) - I^n\bar{d}(\mathbf{g},t|\mathbf{s})^{obs}\right]^2, \\ &= \frac{1}{2}\sum_{s,g}\int dt\left[\Delta\bar{d}(\mathbf{g},t|\mathbf{s})\right]^2, \end{aligned} \tag{1}$$

where $\Delta\bar{d}(\mathbf{g},t|\mathbf{s}) = I^n\bar{d}(\mathbf{g},t|\mathbf{s}) - I^n\bar{d}(\mathbf{g},t|\mathbf{s})^{obs}$ is the data residual, I^n is an integration opertor $I = \int dt$, and n indicates integration performed n times, and $\bar{d}(\mathbf{g},\mathbf{s},t)$ and $\bar{d}(\mathbf{g},\mathbf{s},t)^{obs}$ are predicted and observed modified traces for a point source at $\mathbf{s}$ and a geophone at $\mathbf{g}$.

The modified predicted $\bar{d}(\mathbf{g},t|\mathbf{s})$ and observed $\bar{d}(\mathbf{g},t|\mathbf{s})^{obs}$ traces are obtained by the following equation:

$$\begin{aligned}\bar{d}(\mathbf{g},t|\mathbf{s}) &= \mathcal{F}^{-1}\{L(\omega)|D(\mathbf{g},\mathbf{s})^{obs}|e^{i\phi(\mathbf{g},\mathbf{s})}\},\\ \bar{d}(\mathbf{g},t|\mathbf{s})^{obs} &= \mathcal{F}^{-1}\{L(\omega)|D(\mathbf{g},\mathbf{s})^{obs}|e^{i\phi(\mathbf{g},\mathbf{s})^{obs}}\}. \quad (2)\end{aligned}$$

where $\mathcal{F}^{-1}$ is the inverse Fourier transform and $L(\omega)$ is a low-pass filter. $|D|$ is the magitude spectrum and ϕ is the phase spectrum that are obtained by the Fourier transform of the predicted data $d(\mathbf{g},t|\mathbf{s})$ and observed data $d(\mathbf{g},t|\mathbf{s})^{obs}$ as following

$$\begin{aligned}\mathcal{F}\left[d(\mathbf{g},t|\mathbf{s})\right] &= |D(\mathbf{g},\mathbf{s})|e^{i\phi(\mathbf{g},\mathbf{s})},\\ \mathcal{F}\left[d(\mathbf{g},t|\mathbf{s})^{obs}\right] &= |D(\mathbf{g},\mathbf{s})^{obs}|e^{i\phi(\mathbf{g},\mathbf{s})^{obs}}. \quad (3)\end{aligned}$$

The decoupled P-wave equation for vertical transverse isotropic (VTI) media in the time and wavenumber domain is given by (Zhan et al., 2012)

$$\frac{1}{v_{p_0}^2}\frac{\partial^2 P}{\partial t^2} = -\left[(1+2\epsilon)k_x^2 + k_z^2 - \frac{2(\epsilon-\delta)k_x^2k_z^2}{k_x^2+k_z^2}\right]P, \quad (4)$$

where k_x and k_z are the spatial wavenumber corresponding to point $\mathbf{x}$. The anisotropic parameters $m(\mathbf{x}) \sim (v_{p0},\epsilon,\delta)$ can be estimated using any gradient-based method. To update the anisotropic parameters, the steepest descent method gives

$$m(\mathbf{x})^{(iter+1)} = m(\mathbf{x})^{(iter)} - \alpha\sum_{s,g}\Delta\bar{d}(\mathbf{g},t|\mathbf{s})\frac{\partial I^n\bar{d}(\mathbf{g},t|\mathbf{s})}{\partial m(\mathbf{x})}, \quad (5)$$

where α is the step length and $iter$ is the iteration index.

The phase inversion gradient is calculated by the cross-correlation of the forward-propagated $\bar{p}(\mathbf{x},t|\mathbf{s},0)$ and the backward-propagated wavefield $\bar{g}(\mathbf{x},t|\mathbf{g},0)$ of the residual $\Delta\bar{d}(\mathbf{g},t|\mathbf{s})$. The gradients of the misfit function with respect to the three anisotropy parameters v_{p0}, ϵ and δ.

$$\begin{aligned}\gamma_{v_{p0}}^{mpi}(\mathbf{x}) &= \sum_{s,g}\int_0^T dt\left[\frac{2}{v_{p0}^3(\mathbf{x})}I^n\dot{\bar{g}}(\mathbf{x},t|\mathbf{g},0)\star I^n\dot{\bar{p}}(\mathbf{x},t|\mathbf{s},0)\right]\\ \gamma_{\epsilon}^{mpi}(\mathbf{x}) &= \sum_{s,g}\int_0^T dt\left[I^n\bar{g}(\mathbf{x},t|\mathbf{g},0)\star I^n\bar{U}(\mathbf{x},t|\mathbf{s},0)\right]\\ \gamma_{\delta}^{mpi}(\mathbf{x}) &= \sum_{s,g}\int_0^T dt\left[I^n\bar{g}(\mathbf{x},t|\mathbf{g},0)\star I^n\bar{V}(\mathbf{x},t|\mathbf{s},0)\right]\end{aligned} \quad (6)$$

where $\star$ denotes the temporal convolution, $\bar{U}$ and $\bar{V}$ are given in following.

$$\begin{aligned}\bar{U}(\mathbf{x},t|\mathbf{s},0) &= -2\mathcal{F}^{-1}\left(\frac{k_x^4}{k_x^2+k_z^2}\right)*\bar{p}(\mathbf{x},t|\mathbf{s},0),\\ \bar{V}(\mathbf{x},t|\mathbf{s},0) &= -2\mathcal{F}^{-1}\left(\frac{k_x^2k_z^2}{k_x^2+k_z^2}\right)*\bar{p}(\mathbf{x},t|\mathbf{s},0), \quad (7)\end{aligned}$$

where $\star$ denotes the spatial convolution.

WORKFLOW

The workflow of the multiscale phase inversion is shown in Figure 1. The predicted and recorded data are filtered into different frequency bands by applying different bandpass filters. We start with the data with lower freqenciey contents. The data are integrated N times in the time domain to boost the low-frequency components. The low-boost data are inverted till the misfit change is less than a misfit threshold (ϵ_1). Then the integration times decease by 1. When the integration time is less than 0, the data will be appended with higher frequency content and the MPI procedure is repeated.

SYNTHETIC TESTS

The observed and predicted data are simulated by the rapid expansion method (REM) (Pestana et al., 2011) based on the pesudo-acoustic P-wave VTI wave-equation in equation 4. δ cannot be accurately recovered from such data (Cheng et al., 2014), because surface seismic data are weakly sensitive to variations in the anisotropic parameter δ. Thus δ is set to 0 in the test.

Marmousi Model

An anisotropic marmousi model is shown in Figure 2, where the model size is 4.6 km in the X direction and 2.84 km in the Z direction with a grid spacing of 10 m. One hundred and fifteen sources are located on the surface with a spacing of 40 m, and the traces are recorded by 460 receivers spaced at an interval of 10 m on the free surface. The source wavelet is a Ricker wavelet with a peak frequency of 15 Hz.

We invert for v_{p0} using the true ϵ and δ models. The initial model is shown in Figure 3. The maximal integration time is equal to 2. Five different bandpass filters are applied to the data (see Table 1). Multiscale anisotropic and isotropic phase inversion are applied and the inversion results are shown in Figure 4. The anisotropic phase inversion tomograms is in consistent with the true model. However, the quality of isotropic phase tomogram is poor since the kinematics of the waves are affected by anisotropic effect. The RTM images constructed from anisotropic and isotropic tomograms are shown in Figure 5. In the isotropic RTM image, the reflectors below the anisotropic anormaly are located in the wrong position.

CONCLUSION

In an anisotropic medium, phase information may be strongly influenced by anisotropy. As a result, the erroneous velocity model will lead to a mis-positioning of the reflectors when using isotropic approximation. To avoid this problem, anisotropic effect must be taken into phase inversion.

Multiscale phase inversion (MPI) can be used to invert for the anisotropic parameters from anisotropic data. The velocity structure can be inverted correctly by a single

Table 1: Frequency bands of bandpass filters

Bandpass	f1	f2	f3	f4
1	0.1 Hz	1.1 Hz	5.0 Hz	6.5 Hz
2	4.0 Hz	5.0 Hz	9.0 Hz	10.5 Hz
3	6.0 Hz	7.0 Hz	13.0 Hz	14.5 Hz
4	8.0 Hz	9.0 Hz	19.0 Hz	20.5 Hz
5	12.0 Hz	13.0 Hz	50.0 Hz	51.5 Hz

parameter inversion if an accurate estimate of the δ and ϵ models is known.

ACKNOWLEDGEMENTS

The research reported in this publication was supported by the King Abdullah University of Science and Technology (KAUST) in Thuwal, Saudi Arabia. We are grateful to the sponsors of the Center for Subsurface Imaging and Modeling Consortium for their financial support. For computer time, this research used the resources of the Supercomputing Laboratory at KAUST and the IT Research Computing Group. We thank them for providing the computational resources required for carrying out this work.

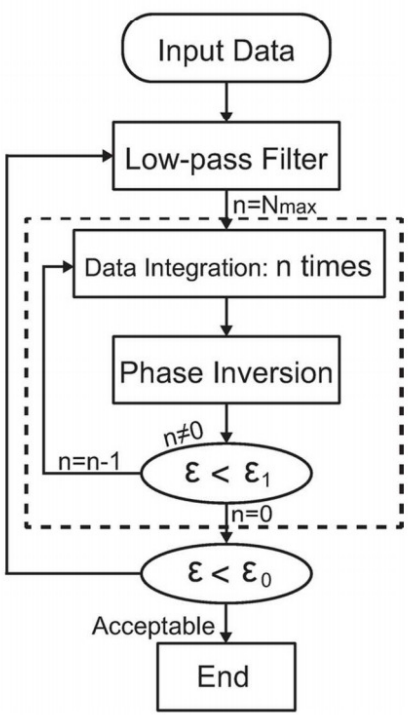

Figure 1: The workflow of multiscale phase inversion. Images adapted from (Fu et al., 2017)

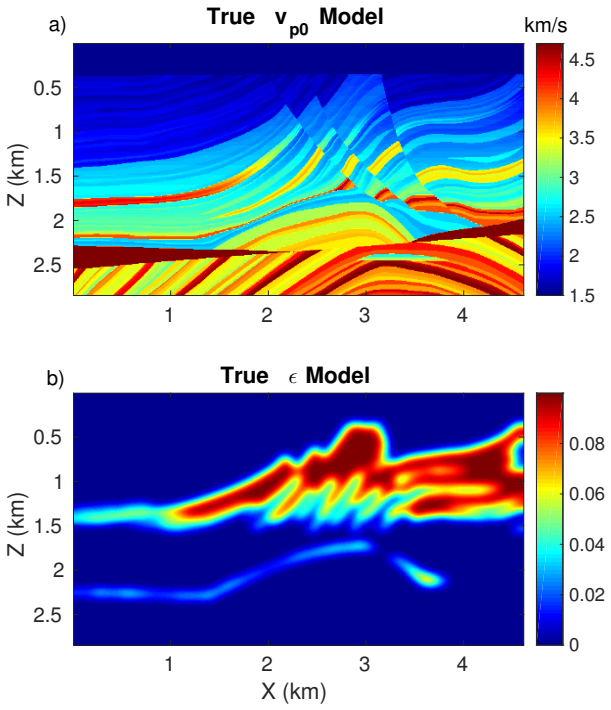

Figure 2: a) The true v_{p0} and b) ϵ models for the Marmousi tests.

REFERENCES

Bunks, C., F. Saleck, S. Zaleski, and G. Chavent, 1995, Multiscale seismic waveform inversion: Geophysics, **60**, 1457–1473.

Cheng, X., K. Jiao, D. Sun, and D. Vigh, 2014, Anisotropic parameter estimation with full-waveform inversion of surface seismic data, *in* SEG Technical Program Expanded Abstracts 2014: Society of Exploration Geophysicists, 1072–1077.

Fu, L., B. Guo, Y. Sun, and G. T. Schuster, 2017, Multiscale phase inversion of seismic data: Geophysics, **83**, 1–52.

Luo, Y., and G. T. Schuster, 1991a, Wave equation inversion of skeletalized geophysical data: Geophysical Journal International, **105**, 289–294.

———, 1991b, Wave-equation traveltime inversion: Geophysics, **56**, 645–653.

Ma, Y., and D. Hale, 2013, Wave-equation reflection traveltime inversion with dynamic warping and full-waveform inversion: Geophysics, **78**, R223–R233.

Pestana, R. C., B. Ursin, and P. L. Stoffa, 2011, Separate P-and SV-wave equations for VTI media: Presented at the 12th International Congress of the Brazilian Geophysical Society.

Sava, P., and I. Vlad, 2008, Numeric implementation of wave-equation migration velocity analysis operators: Geophysics, **73**, VE145–VE159.

Sava, P. C., B. Biondi, and J. Etgen, 2005, Wave-equation migration velocity analysis by focusing diffractions and reflections: Geophysics, **70**, U19–U27.

Shihang, F., et al., 2017, Skeletonized wave-equation inversion in vertical symmetry axis media without too much math: Interpretation, **78**, SO21–SO30.

Sun, Y., and G. T. Schuster, 1993, Time-domain phase

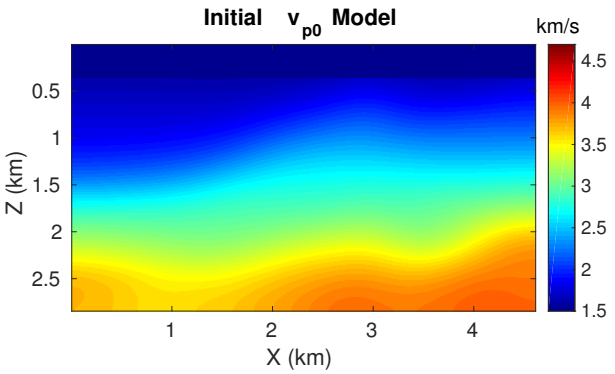

Figure 3: The initial v_{p0} model for the Marmousi tests

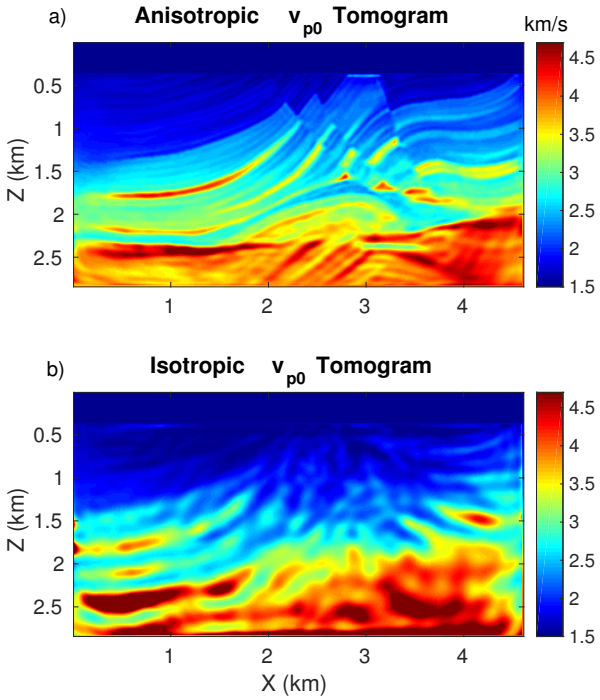

Figure 4: a) The v_{p0} tomograms after 50 iterations of multiscale anisotropic phase inversion. b) The v_{p0} tomograms after 50 iterations of multiscale isotropic phase inversion.

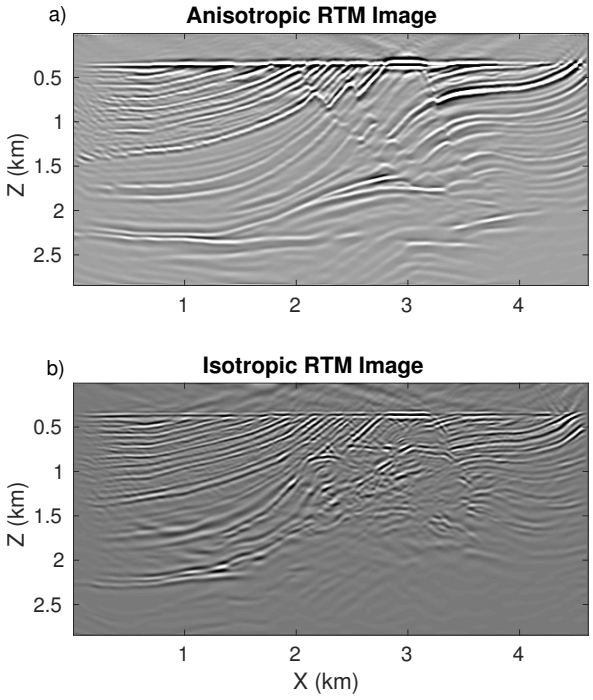

Figure 5: a) Anisotropic RTM image with anisotropic v_{p0} tomograms. b) Isotropic RTM image with isotropic v_{p0} tomograms.

inversion, *in* SEG Technical Program Expanded Abstracts 1993: Society of Exploration Geophysicists, 684–687.

Tarantola, A., 2005, Inverse problem theory and methods for model parameter estimation: siam.

Virieux, J., and S. Operto, 2009, An overview of full-waveform inversion in exploration geophysics: Geophysics, **74**, WCC1–WCC26.

Zhan, G., R. C. Pestana, and P. L. Stoffa, 2012, Decoupled equations for reverse time migration in tilted transversely isotropic media: Geophysics, **77**, T37–T45.

Zhou, C., W. Cai, Y. Luo, G. T. Schuster, and S. Hassanzadeh, 1995, Acoustic wave-equation traveltime and waveform inversion of crosshole seismic data: Geophysics, **60**, 765–773.